December, 2001

Antilambda production in Au+Au collisions at 11.7A GeV/c

B. B. Back, *Argonne National Laboratory*
R. R. Betts, *University of Illinois at Chicago*
J. Chang, *University of California, Riverside*
C. Y. Chi, *Columbia University*
Y. Y. Chu, *Brookhaven National Laboratory*, et al.

Antilambda Production in Au + Au Collisions at 11.7A GeV/c

B. B. Back,[1] R. R. Betts,[1,2] J. Chang,[3] W. C. Chang,[3] C. Y. Chi,[4] Y. Y. Chu,[5] J. B. Cumming,[5] J. C. Dunlop,[6] W. Eldredge,[3] S. Y. Fung,[3] R. Ganz,[2] E. Garcia,[7] A. Gillitzer,[1] G. Heintzelman,[6] W. F. Henning,[1] D. J. Hofman,[2] B. Holzman,[2] J. H. Kang,[8] E. J. Kim,[8] S. Y. Kim,[8] Y. Kwon,[8] D. McLeod,[2] A. C. Mignerey,[7] M. Moulson,[4] V. Nanal,[1] C. A. Ogilvie,[6] R. Pak,[9] A. Ruangma,[7] D. E. Russ,[7] R. Seto,[3] P. J. Stanskas,[7] G. S. F. Stephans,[6] H. Wang,[3] F. L. H. Wolfs,[9] A. H. Wuosmaa,[1] H. Xiang,[3] G. H. Xu,[3] H. B. Yao,[6] and C. M. Zou[3]

(The E917 Collaboration)

[1]*Argonne National Laboratory, Argonne, Illinois 60439*
[2]*University of Illinois at Chicago, Chicago, Illinois 60607*
[3]*University of California Riverside, Riverside, California 92521*
[4]*Columbia University, Nevis Laboratory, Irvington, New York 10533*
[5]*Brookhaven National Laboratory, Upton, New York 11973*
[6]*Massachusetts Institute of Technology, Cambridge, Massachusetts 02139*
[7]*University of Maryland, College Park, Maryland 20742*
[8]*Yonsei University, Seoul 120-749, South Korea*
[9]*University of Rochester, Rochester, New York 14627*

(Received 23 January 2001; published 19 November 2001)

We present results for antilambda and antiproton production in Au + Au collisions at 11.7 A GeV/c including spectra and extracted invariant yields for both species in central and peripheral collisions in the rapidity range $1.0 < y < 1.4$. The antilambda yield increases from $dN_{\bar{\Lambda}}/dy = 1.2^{+0.7+0.2}_{-0.6-0.2} \times 10^{-3}$ in peripheral collisions to $19^{+4+3}_{-5-2} \times 10^{-3}$ in central collisions. The direct antiproton yield is deduced from the measured total antiproton spectra to extract the ratio of antilambda-to-direct-antiproton production. The $\bar{\Lambda}/\bar{p}$ ratio near midrapidity increases from $0.26^{+0.19+0.5}_{-0.15-0.4}$ in peripheral collisions to $3.6^{+4.7+2.7}_{-1.8-1.1}$ in central collisions, a value larger than current theoretical estimates.

DOI: 10.1103/PhysRevLett.87.242301 PACS numbers: 25.75.–q, 13.85.Ni, 21.65.+f

Enhanced antimatter and strangeness production have both been proposed as signatures of the phase transition from normal hadronic matter to the quark-gluon plasma (QGP) [1–3]. The yields of strange antibaryons combine both of these signatures in a single production channel, and may prove to be a particularly sensitive probe for the formation of the QGP. Of particular interest is the ratio $\bar{\Lambda}/\bar{p}$ [1], which reflects the relative abundance of $\bar{s}$ quarks to light antiquarks.

However, both $\bar{\Lambda}$ and $\bar{p}$ are also produced when the collision does not form a QGP. Hadronic matter with sufficient rescattering can reach a chemical equilibrium containing the full spectrum of hadrons. Equilibrium chemical models of heavy-ion collisions are generally able to reproduce the measured ratios of total yields of particles such as pions and kaons. Such models also predict values for the ratio $\bar{\Lambda}/\bar{p}$ in the range 0.15–0.9 at AGS beam energies [4,5]. A thermal model analysis that accounts for the measured K^+/π^+ and K^-/K^+ ratios [6] gives a most probable value of $\bar{\Lambda}/\bar{p} = 1$, with unrealistic values yielding an upper limit of 2 for Au + Au collisions.

Hadronic cascade models that explicitly follow the reactions and trajectories of hadrons in the collision zone [7,8] predict values for the $\bar{\Lambda}/\bar{p}$ ratio of approximately 1. The absorption cross section for $\bar{\Lambda}$-N processes is not well known at these energies, opening the possibility for differential absorption of the two species to play a role in determining the value of the ratio $\bar{\Lambda}/\bar{p}$ and its rapidity dependence. However, a study has shown that a reasonable interpretation of this value cannot bring the predictions of cascade models above a ratio of ~1 [6]. Recent data from E877 on the antiflow of $\bar{p}$ [9] are successfully described by the hadronic cascades that use the normal antiproton annihilation cross section.

Enhanced antibaryon production may also be due to many-body collisions between pions, e.g., $n\pi \rightarrow \bar{p} + p$ [10,11]. The rate of antibaryon production can be estimated from the inverse reaction $\bar{p} + p \rightarrow n\pi$. Calculations by Rapp [10] and Greiner [11] indicate that a significant number of both $\bar{p}$ and $\bar{\Lambda}$ may come from these processes, but it is not yet clear how to incorporate these many-body collisions into current hadronic cascade calculations.

In summary, hadronic models with reasonable inputs generally predict $\bar{\Lambda}/\bar{p} \leq 1$. Thus the experimental detection of a $\bar{\Lambda}/\bar{p}$ ratio significantly larger than 1 may signal the breakdown of these hadronic models, and possibly the onset of other degrees of freedom in the system. Of particular interest is the centrality dependence of the $\bar{\Lambda}/\bar{p}$ ratio, which may discriminate [12] between the various models attempting to describe antibaryon production: QGP, hadronic scattering, and thermal models. Canonical thermal models should be used in this comparison, since the volume of the emitting system has been shown to affect the ratio of strange to nonstrange particles by up to a factor of 4 [13].

There are indications of an abnormally large value of the $\bar{\Lambda}/\bar{p}$ ratio from other experiments. Experiment E859 reported a directly measured $\bar{\Lambda}/\bar{p}$ ratio of $2.9 \pm 0.9(\text{stat}) \pm 0.5(\text{sys})$ near midrapidity in central Si + Au collisions, at a beam energy of $14.6A$ GeV/c [14]. An indirect estimate of $\bar{\Lambda}/\bar{p} > 2.3$ (98% C.L.) at $y = 1.6$ for $p_\perp \sim 0$ in central Au + Pb collisions was obtained at a beam energy of $11.5A$ GeV/c by comparing inclusive antiproton yields from two different experiments (E864 and E878) with largely different acceptances [15].

In this Letter, we present a determination of $\bar{\Lambda}$ yields in Au + Au collisions near midrapidity and over an extended range in $p_\perp$. We also measure the total $\bar{p}$ spectrum, which includes contributions from both direct $\bar{p}$ production and $\bar{\Lambda}$ decay.

The experiment was carried out using the magnetic tracking spectrometer previously employed in AGS experiments E802, E859, and E866 as described in detail in Refs. [16–19]. An efficient second-level trigger was used in order to study the production of rare particles such as antiprotons. A ^{197}Au beam with momentum $11.7A$ GeV/c was incident on a 1-g/cm^2-thick Au target. The movable spectrometer subtended polar angles from 19° to 34°. Magnetic field settings of ± 0.4 T were used, for which the momentum resolution of the spectrometer, $\delta p/p$, ranges from 1% to 2%. At these angle and field settings, we have acceptance for $\bar{p}$ and $\bar{\Lambda}$ in the rapidity range $1.0 < y < 1.4$, where midrapidity is $y = 1.6$ at this beam energy. Particle identification is based on the measured momentum combined with a time-of-flight (TOF) wall with a resolution of 135 ps situated 6 m from the target.

Using the total kinetic energy of spectator particles measured in a zero-degree calorimeter, the data were divided into two centrality classes, called "central" and "peripheral," containing 0%–12% and 12%–77% of σ_{tot} (=6.8 b [20]), respectively.

The reconstruction, particle identification, and tracking algorithms have been described in detail elsewhere [18]. Antiprotons are accepted up to momentum 2.9 GeV/c, above which the 3σ identification bands of the K^- and $\bar{p}$ time-of-flight spectrum begin to overlap. A lower momentum cutoff of 0.5 GeV/c was necessitated by hadronic interaction rates in the spectrometer material. Pions used to reconstruct $\bar{\Lambda}$'s were required to have momenta between 0.35–1.8 GeV/c. The $\bar{p}$ and $\bar{\Lambda}$ results are from the same data sample.

A firm understanding of the background in the TOF-identified $\bar{p}$ sample is required for the measurement of the $\bar{p}$ spectrum. Spectra of the time-of-flight residuals $\Delta t = (t_{\text{meas}} - t_{\text{expected}})/\sigma$ were created in order to estimate these backgrounds in the $\bar{p}$ sample. Here t_{meas} and t_{expected} are the measured and expected flight times of $\bar{p}$'s to the TOF wall, and σ is a particle-by-particle estimate of the timing resolution based on the TOF wall resolution combined with a Monte Carlo simulation of the tracking in the spectrometer. The Δt distributions are parametrized by a Gaussian for the true $\bar{p}$ signal and a background with two components: an exponentially falling contribution from the tails of K^- and π^- bands, and a flat random contribution due to misidentified particles. The backgrounds extracted range from 15% to 75% of the total signal, with the largest backgrounds at the extremes of the momentum ranges. Rapidity-transverse mass bins for which the background fraction exceeds 50% have been excluded from further analysis.

The counting statistics in determining the background are included in the reported statistical errors. We estimate an additional systematic error in the extracted $\bar{p}$ yield due to background corrections and acceptance uncertainties to be 10%, and the error in the $\bar{p}$ inverse slope, arising mostly from acceptance uncertainties, to be 5%. The measured $\bar{p}$ invariant spectra are shown as open circles in Fig. 1 as a function of transverse mass ($m_\perp = \sqrt{p_\perp^2 + m_0^2}$), along with independent fits (dashed lines) of a standard Boltzmann form [21], $B(T)$; i.e.,

$$\frac{1}{2\pi m_\perp}\frac{d^2N}{dm_\perp dy} = \frac{dN}{dy}B(T) = \frac{dN}{dy}\frac{1}{2\pi}m_\perp\frac{\exp[-(m_\perp - m_0)/T]}{m_0^2T + 2m_0T^2 + 2T^3}.$$

The parameters of the fit to the total $\bar{p}$ spectra ($dN_{\bar{p}\text{total}}/dy, T_{\bar{p}\text{total}}$) are given in columns two and three of Table I and are in good agreement with [22]. These spectra include contributions from both direct production ($\bar{p}_{\text{direct}}$) and antihyperon decay ($\bar{p}_{\text{decay}}$), which we now consider.

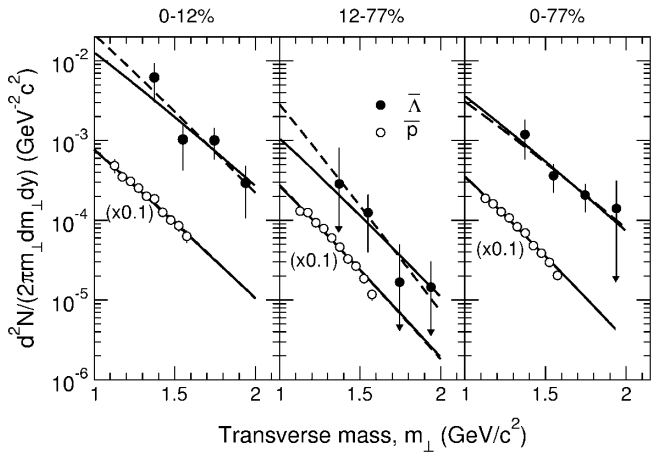

FIG. 1. Invariant yields as a function of transverse mass for $\bar{\Lambda}$ (solid circles) and total $\bar{p}$ (open circles, multiplied by 0.1 for clarity) in the three centrality classes. The error bars include a 2% point-to-point systematic error due to acceptance corrections, and an arrow on the bottom error bar is to indicate it extends below the plot limits. The solid lines are from the simultaneous fit as described in the text and the dashed lines are from independent fits to $\bar{\Lambda}$ and $\bar{p}$ data shown for comparison. Solid and dashed fit lines overlap for the $\bar{p}$ spectra.

TABLE I. Parameters of an independent fit to the total measured $\bar{p}$ spectrum ($dN_{\bar{p}\text{total}}/dy, T_{\bar{p}\text{total}}$) and a simultaneous fit (the remaining values) to $\bar{p}$ and $\bar{\Lambda}$ data, for the three centrality bins. See text for an explanation of the parameters. Errors are statistical followed by systematic.

Bin	$dN_{\bar{p}\text{total}}/dy$ ($\times 10^{-3}$)	$T_{\bar{p}\text{total}}$ (GeV)	$T_{\bar{p}\text{direct}}$ (GeV)	$dN_{\bar{\Lambda}}/dy$ ($\times 10^{-3}$)	$T_{\bar{\Lambda}}$ (GeV)	$\bar{\Lambda}/\bar{p}_{\text{direct}}$
0%–12%	$17.7 \pm 0.5 \pm 1.8$	$0.200 \pm 0.008 \pm 0.010$	$0.23^{+0.15+0.1}_{-0.06-0.01}$	19^{+4+3}_{-5-2}	$0.22^{+0.04+0.01}_{-0.03-0.01}$	$3.6^{+4.7+2.7}_{-1.8-1.1}$
12%–77%	$5.5 \pm 0.1 \pm 0.6$	$0.175 \pm 0.004 \pm 0.008$	$0.18^{+0.02+0.01}_{-0.01-0.01}$	$1.2^{+0.7+0.2}_{-0.6-0.2}$	$0.19^{+0.06+0.01}_{-0.03-0.01}$	$0.26^{+0.19+0.5}_{-0.15-0.4}$
0%–77%	$7.4 \pm 0.1 \pm 0.7$	$0.185 \pm 0.004 \pm 0.009$	$0.183^{+0.017+0.014}_{-0.014-0.003}$	$5.3^{+1.1+1.0}_{-1.1-1.0}$	$0.218^{+0.026+0.020}_{-0.020-0.004}$	$1.3^{+0.6+0.6}_{-0.4-0.3}$

We reconstruct $\bar{\Lambda}$'s through direct measurement of $(\bar{p}, \pi^+)$ pairs. This decay channel has a branching ratio of 63.9% [23]. The spectrum of reconstructed invariant mass for accepted $(\bar{p}, \pi^+)$ pairs is shown in Fig. 2. The experimental resolution for reconstructing $\bar{\Lambda}$'s is found by initially reconstructing the Λ invariant mass spectrum in the same data set. The peak of the Λ spectrum is found to be at 1.1161 ± 0.0004 GeV/c^2, consistent with the accepted value of $m_\Lambda = 1.1157$ GeV/c^2. The Gaussian width of the peak is $\sigma = 1.3$ MeV/c^2, which is attributable to experimental resolution. To define $\bar{\Lambda}$ candidates, a cut of $\pm 3\sigma$ is taken around the nominal m_Λ. To estimate the background under the $\bar{\Lambda}$ peak, we have constructed a mixed-event background, shown as the solid histogram in Fig. 2. Pairs are constructed by selecting random $\bar{p}$'s and π^+'s from the set of all pairs in the centrality class being considered. The background is normalized to the region outside the $\bar{\Lambda}$ peak, defined as more than 6σ from m_Λ. Both real and mixed pairs were included only if their opening angle was greater than 15 mrad. This removes most of the inefficiency for detecting close tracks. The remaining two-track inefficiency is estimated by comparison with the mixed-event sample. The correction is then applied on a pair-by-pair basis in generating the background invariant mass spectrum and the signal's final $m_\perp$ binned yields. This correction has less than a 5% effect on the yields.

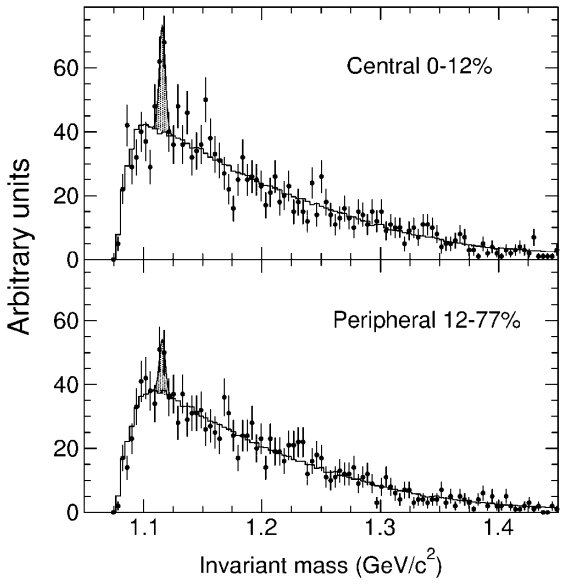

FIG. 2. The $\bar{\Lambda}$ invariant mass data for central and peripheral collisions for the data in Fig. 1 ($1.0 < y < 1.4$). Solid points are measured data, and the histogram is the normalized mixed-event background after all corrections have been applied. The $\bar{\Lambda}$ mass peak is shaded for visual clarity only.

We further correct the estimated background for the residual correlations arising from the presence of particles from signal pairs in the mixed-event background. Pairs in the mixed-event background with a member that came from the signal region are assigned a weight equal to the background fraction. This must be done in an iterative fashion; four iterations are sufficient to attain convergence. This correction increases the extracted $\bar{\Lambda}$ yields by approximately 15%. From the small remaining discrepancy between the shape of the mixed-event sample and the actual sample, we estimate the systematic error on the measured $\bar{\Lambda}$ yield arising from background subtraction to be 15%. The $\bar{\Lambda}$ invariant yields are shown as solid circles in Fig. 1 binned as a function of transverse mass in all centrality classes.

Since the $\bar{p}$ spectra have a strong contribution from $\bar{\Lambda}$ decays, it is advantageous, and for the peripheral sample crucial due to limited $\bar{\Lambda}$ decays, to perform a simultaneous fit to both data sets in order to obtain the most accurate measure of the $\bar{\Lambda}/\bar{p}$ ratio. The $\bar{\Lambda}$ and $\bar{p}$ transverse mass data were therefore fit simultaneously using the functions

$$\frac{1}{2\pi m_\perp}\frac{d^2N_{\bar{\Lambda}}}{dm_\perp dy} = \frac{dN_{\bar{\Lambda}}}{dy}B(T_{\bar{\Lambda}}), \qquad \text{and}$$

$$\frac{1}{2\pi m_\perp}\frac{d^2N_{\bar{p}}}{dm_\perp dy} = \frac{dN_{\bar{\Lambda}}}{dy}\left(\frac{B(T_{\bar{p}\text{direct}})}{\bar{\Lambda}/\bar{p}_{\text{direct}}} + 0.639B(T_{\bar{p}\text{decay}})\right),$$

where $T_{\bar{p}\text{decay}} = 0.834T_{\bar{\Lambda}} + 0.004$ (GeV) as found in a Monte Carlo study to parametrize the distribution of $\bar{p}$'s originating from $\bar{\Lambda}$ decay. From these fits, shown in Fig. 1, we obtain values of the four free parameters $T_{\bar{p}\text{direct}}$, $dN_{\bar{\Lambda}}/dy$, $T_{\bar{\Lambda}}$, and $\bar{\Lambda}/\bar{p}_{\text{direct}}$, listed in Table I. The $\bar{\Lambda}/\bar{p}$ ratio and $\bar{\Lambda}$ yield obtained in this manner are consistent with the lower precision result obtained from separate fits to the $\bar{\Lambda}$ and $\bar{p}$ data [24].

In summary, we have made a direct determination of $\bar{\Lambda}$ production in Au + Au collisions at the AGS. We find that the $\bar{\Lambda}$ production increases sharply with centrality, from $dN_{\bar{\Lambda}}/dy = 1.2^{+0.7+0.2}_{-0.6-0.2} \times 10^{-3}$ in peripheral collisions to

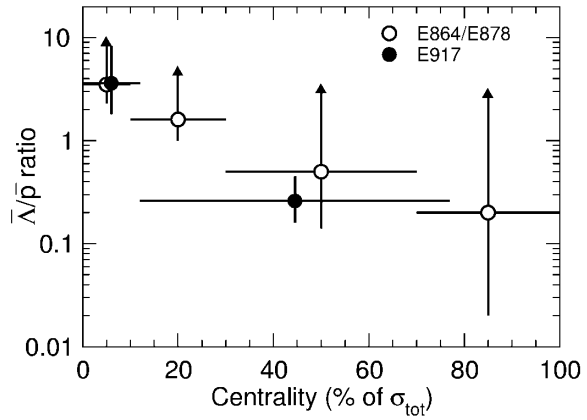

FIG. 3. The $\bar{\Lambda}/\bar{p}$ ratio is shown as a function of the centrality given in terms of the percentage of the total interaction cross section, σ_{tot}. The E917 data are integrated over all $p_\perp$ and $1.0 < y < 1.4$ and are shown as solid circles with 1σ statistical error bars for the $\bar{\Lambda}/\bar{p}$ ratio. The E864/E878 indirect results are at $p_\perp \sim 0$ and $y = 1.6$ and are shown as most probable values with the 98% confidence level of the minimum value indicated by the lower error bar. Upper limits are not given. Horizontal bars indicate bin widths.

$19^{+4+3}_{-5-2} \times 10^{-3}$ in central collisions. The total $\bar{p}$ production is of comparable magnitude to the $\bar{\Lambda}$ yield, with a substantial fraction of the measured $\bar{p}$ signal attributable to decay products from the $\bar{\Lambda}$.

We find that the ratio $\bar{\Lambda}/\bar{p}_{\text{direct}}$ near midrapidity increases from $0.26^{+0.19+0.5}_{-0.15-0.4}$ in peripheral collisions to $3.6^{+4.7+2.7}_{-1.8-1.1}$ in central collisions. When combined with the prior observations of elevated ratios in central Si + Au collisions [14] and the indirect evidence from experiments E864 and E878 [15], the present results indicate that $\bar{\Lambda}$ production is larger than direct $\bar{p}$ production in central collisions — and not in peripheral collisions — at AGS beam energies. This effect is clearly shown in Fig. 3. The mechanism responsible for the large $\bar{\Lambda}/\bar{p}$ ratio is currently unknown.

This work is supported by the U.S. Department of Energy under contracts with ANL (No. W-31-109-ENG-38), BNL (No. DE-AC02-98CH10886), MIT (No. DE-AC02-76ER03069), UC Riverside (No. DE-FG03-86ER40271), UIC (No. DE-FG02-94ER40865) and the University of Maryland (No. DE-FG02-93ER40802), the National Science Foundation under contract with the University of Rochester (No. PHY-9722606), and the Ministry of Education and KOSEF (No. 951-0202-032-2) in Korea.

[1] J. Rafelski and B. Mueller, Phys. Rev. Lett. **48**, 1066 (1982); **56**, 2334(E) (1982).
[2] J. Rafelski, Phys. Rep. **88**, 331 (1982).
[3] P. Koch, B. Mueller, and J. Rafelski, Phys. Rep. **142**, 167 (1986).
[4] J. Rafelski and M. Danos, Phys. Rev. C **50**, 1684 (1994).
[5] F. Becattini *et al.,* hep-ph/0002267. The $\bar{\Lambda}/\bar{p}$ ratio is estimated here by assuming the calculated yield of lambda equals the calculated yield of K^+, multiplying quoted ratios, and correcting for $\bar{\Lambda}$ feed-down.
[6] G. J. Wang, G. Welke, R. Bellwied, and C. Pruneau, *Advances in Nuclear Dynamics 4,* edited by W. Bauer and H. G. Ritter (Plenum, New York, 1998), pp. 369–378; nucl-th/9807036.
[7] Review articles on transport models [8] state that the models underpredict by a factor of 3–5 the measured Si + Au ratio of $\bar{\Lambda}/\bar{p} = 2.9 \pm 0.9 \pm 0.5$. Wang [J. Phys. G, Nucl. Part. Phys. **27**, 283 (2001); (private communication)] estimates a $\bar{\Lambda}/\bar{p}$ ratio ~1.3 at nonzero $p_\perp$ for central Au + Au collisions at AGS energies.
[8] S. Bass *et al.,* J. Phys. G, Nucl. Part. Phys. **25**, R1 (1999).
[9] J. Barrette *et al.,* Phys. Lett. B **485**, 319 (2000).
[10] R. Rapp and E. Shuryak, hep-ph/0008326.
[11] C. Greiner and S. Leupold, nucl-th/0009036.
[12] M. Bleicher *et al.,* Phys. Rev. C **59**, R1844 (1999).
[13] S. Hamieh *et al.,* Phys. Lett. B **486**, 61 (2000).
[14] E859 Collaboration, G. S. F. Stephans *et al.,* J. Phys. G, Nucl. Part. Phys. **23**, 1895 (1997).
[15] E864 Collaboration, T. A. Armstrong *et al.,* Phys. Rev. C **59**, 2699 (1999).
[16] T. Abbott *et al.,* Nucl. Instrum. Methods Phys. Res., Sect. A **290**, 41 (1990).
[17] L. Ahle *et al.,* Phys. Rev. C **57**, R466 (1998).
[18] L. Ahle *et al.,* Phys. Rev. C **58**, 3523 (1998).
[19] L. Ahle *et al.,* Phys. Lett. B **476**, 1 (2000).
[20] L. Y. Geer *et al.,* Phys. Rev. C **52**, 334 (1995).
[21] B. B. Back *et al.,* Phys. Rev. Lett. **86**, 1970 (2001).
[22] L. Ahle *et al.,* Phys. Rev. Lett. **81**, 2650 (1998).
[23] D. E. Grom *et al.,* Eur. Phys. J. C **15**, 1 (2000).
[24] Independent fits to the $\bar{\Lambda}$ data result in $dN_{\bar{\Lambda}}/dy = 24 \pm 9 \pm 4 \times 10^{-3}$, $2 \pm 2 \pm 1 \times 10^{-3}$, and $5 \pm 1.5 \pm 0.8 \times 10^{-3}$ for 0%–12%, 12%–77%, and 0%–77% centrality bins, respectively.